A&A 602, L15 (2017)
DOI: 10.1051/0004-6361/201731018

Astronomy & Astrophysics

Letter to the Editor

Feature-rich transmission spectrum for WASP-127b

Cloud-free skies for the puffiest known super-Neptune?

E. Palle[1,2], G. Chen[1,2,3], J. Prieto-Arranz[1,2], G. Nowak[1,2], F. Murgas[1,2], L. Nortmann[1,2], D. Pollacco[4], K. Lam[4], P. Montanes-Rodriguez[1,2], H. Parviainen[1,2], and N. Casasayas-Barris[1,2]

[1] Instituto de Astrofísica de Canarias, Vía Láctea s/n, 38205 La Laguna, Tenerife, Spain
e-mail: epalle@iac.es
[2] Departamento de Astrofísica, Universidad de La Laguna, 38200 San Cristobâl de La Laguna, Spain
[3] Key Laboratory of Planetary Sciences, Purple Mountain Observatory, Chinese Academy of Sciences, 210008 Nanjing, PR China
[4] Department of Physics, University of Warwick, Coventry CV4 7AL, UK

Received 21 April 2017 / Accepted 22 May 2017

ABSTRACT

Context. WASP-127b is a planet with one of the lowest densities discovered to date. With a sub-Saturn mass ($M_p = 0.18 \pm 0.02\,M_J$) and super-Jupiter radius ($R_p = 1.37 \pm 0.04\,R_J$), it orbits a bright G5 star that is about to leave the main-sequence.
Aims. We aim to explore the atmosphere of WASP-127b in order to retrieve its main atmospheric components, and to find hints for its intriguing inflation and evolutionary history.
Methods. We used the ALFOSC spectrograph at the NOT telescope to observe a low-resolution ($R \sim 330$, seeing limited) long-slit spectroscopic time series during a planetary transit, and present here the first transmission spectrum for WASP-127b.
Results. We find a strong Rayleigh slope at blue wavelengths and a hint of Na absorption, although the quality of the data does not allow us to claim a detection. At redder wavelengths the absorption features of TiO and VO are the best explanation to fit the data.
Conclusions. Although observations with a higher signal-to-noise ratio are needed to conclusively confirm the absorption features, WASP-127b seems to posses a cloud-free atmosphere and is one of the best targets on which to perform further characterization studies in the near future.

Key words. planetary systems – planets and satellites: individual: WASP-127b – planets and satellites: atmospheres – techniques: spectroscopic

1. Introduction

The atmospheres of exoplanets are a unique window for investigating the planetary chemistry, which can help improve our understanding of planetary interior properties and provide links to planet formation and migration histories (e.g., Guillot 2005; Fortney et al. 2007; Fortney & Nettelmann 2010; Öberg et al. 2011; Mousis et al. 2012; Madhusudhan et al. 2014, 2016). Transmission spectroscopy retrieves the absorption and scattering signatures from the atmosphere at the planetary day-night terminator region. These signatures are only imprinted on the stellar light when it is transmitted through the planetary atmosphere during a transit, and they can be extracted through the differential method when they are compared to out-of-transit measurements. Such studies have been carried out by many ground-based large telescopes and space telescopes in a wide range of spectral resolutions (e.g., Charbonneau et al. 2002; Snellen et al. 2010; Bean et al. 2010; Sing et al. 2016), resulting in robust detections of Na, K, H_2O, CO, and scattering hazes (see the inventory listed in Bailey 2014 and Sing et al. 2016). A recent HST+*Spitzer* survey led by Sing et al. (2016) performed a comparative study on ten hot Jupiters covering 0.3−5 μm. This diverse hot-Jupiter sample reveals a continuum from clear to cloudy atmospheres and suggests that clouds or hazes are the cause of weakened spectral features.

As the investigated sample increases, it is fundamental to construct a spectral sequence for exoplanets for a global picture of population characteristics and formation or evolution scenarios, similar to what we have achieved for stars and brown dwarfs. In the near future, the JWST will provide spectral resolutions at high signal-to-noise ratio (S/N) with a large wavelength coverage of 0.6−28 μm that can distinguish among different atmospheric compositions. However, ground-based observations can also complement JWST by extending the wavelength range to $\lambda < 600$ nm, which is critical for examining spectral signatures arising from Rayleigh scattering, Na, or TiO/VO (Murgas et al. 2014; Nortmann et al. 2016; Chen et al. 2017a,c). The ideal starting point are low-density planets, which are more likely to host extended atmospheric envelopes that can produce stronger transmission signals if they are cloud free.

WASP-127b (Lam et al. 2017), with a mass of $0.18 \pm 0.02\,M_J$ and a radius of $1.37 \pm 0.04\,R_J$, is the planet with the puffiest, lowest density discovered to date. It has an orbital period of 4.18 days and orbits a bright parent star ($V = 10.2$), which makes it a very interesting object for atmospheric follow-up studies.

The host star of WASP-127b is a G5 star that is at the end of the main-sequence phase and moving to the sub-giant branch (Lam et al. 2017). Moreover, the unusually large radius (compared to its sub-Saturn mass) cannot be explained by the standard coreless model (e.g., Fortney et al. 2007), and places it in the short-period Neptune desert, a region between Jovian and super-Earth planets with a lack of detected planets (Howard et al. 2012; Mazeh et al. 2016). Several inflation mechanisms have been proposed to explain this inflation, including tidal heating, enhanced atmospheric opacity,

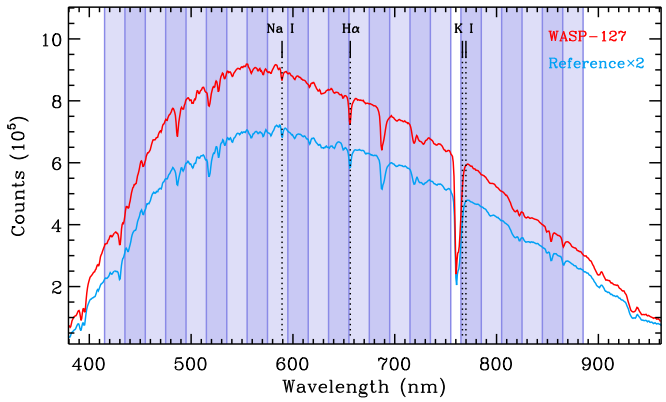

Fig. 1. Example stellar spectra of WASP-127 (red) and the reference star (blue) obtained with grism 4 of NOT/ALFOSC on the night of February 23, 2017. The color-shaded areas indicate the divided passbands that are used to create the spectroscopic light curves. The oxygen *A*-band region is excluded.

Ohmic heating, and/or reinflation by the host star when moving toward the red giant branch phase (Leconte et al. 2010; Batygin & Stevenson 2010; Batygin et al. 2011; Lammer et al. 2013; Rauscher & Menou 2013; Spiegel & Burrows 2013; Wu & Lithwick 2013; Lopez & Fortney 2016), although no concluding observations have been established yet to favor one or the other. The formation and evolution mechanisms of WASP-127b are therfore very intriguing, given its transition size between these two classes of planets.

2. Observations and data reduction

We observed one transit of WASP-127b on the night of February 23, 2017, using the Andalucia Faint Object Spectrograph and Camera (ALFOSC) mounted at the 2.5 m Nordic Optical Telescope (NOT) at ORM observatory. ALFOSC has a field of view of 6.′4 × 6.′4 and a 2048 × 2048 E2V detector with a pixel size of 0.″2. The observation was carried out in long-slit mode using a 40″ wide slit to avoid flux losses, and placing both WASP-127 and a reference star simultaneously aligned in the slit. The reference star TYC 4916-897-1 is located 40.″5 away from WASP-127 and it is about one magnitude fainter (V = 11.2) over the observed spectral range. Grism 4 was used to simultaneously cover the spectral range from 320−960 nm. Observations started at 23:45 UT and ended at 05:36 UT, resulting in a time series of 746 spectra. Exposure times were set to 20 s. The transit of WASP-127b (T_{14}) started at 00:19 UT and ended at 04:38 UT, resulting in 554 spectra taken within transit. The night was clear, with a relatively stable seeing of around 0.″5 during the full observation. The airmass changed from 1.35 to 1.19, then to 2.45.

Data reduction was carried out using the approach outlined in Chen et al. (2017b,a) for similar OSIRIS long-slit data taken with the GTC. The one-dimensional spectra (see Fig. 1) were extracted using the optimal extraction algorithm (Horne 1986) with an aperture diameter of 13 pixels, which minimized the scatter for the white-color light curves created from various trial aperture sizes. The time stamp was centered on mid-exposureand converted into the barycentric dynamical time standard (BJD_{TDB}; Eastman et al. 2010). Misalignment between the target and reference stars in the wavelength solutions and any spectral drifts were corrected. Then the requested wavelength range of a given passband was converted into a pixel range, and the flux was summed to generate the time series.

A broadband (white-color) light curve was integrated from 395 nm to 945 nm, excluding the range of 755−765 nm to eliminate the noise introduced by the oxygen A band (Parviainen et al. 2016), and used to derive the transit parameters in Fig. 2. Moreover, several narrowband light curves were constructed to study the wavelength-dependence of the transit depth and derive the transmission spectrum (see Fig. 1 for the band ranges).

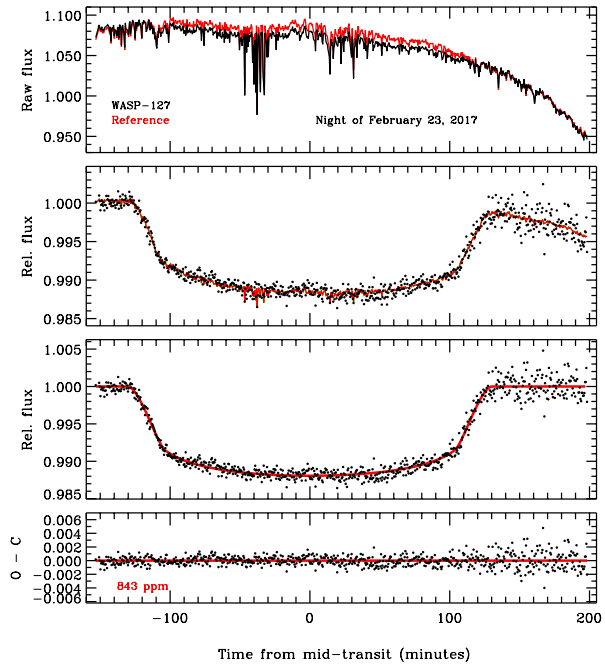

Fig. 2. *Panels from top to bottom*: (1) raw flux of WASP-127 (black line) and the reference star (red line) obtained with ALFOSC at NOT; (2) relative flux between the WASP-127 and the reference star (black dots) and the best-fitting combined model (red line); (3) same as in panel 2, but detrended; (4) best-fitting light-curve residuals.

3. Light-curve analysis

The light-curve data were modeled in the approach detailed in Chen et al. (2017b,a). In brief, the light-curve model contains two multiplicative components. One component describes the astrophysical signal, which adopts the analytic transit model $\mathcal{T}(p)$ proposed by Mandel & Agol (2002). The other component describes the systematics of telluric or instrumental origins in a fully parametric form or in a semi-empirical form, which is designated as the baseline model $\mathcal{B}(c_i)$.

The transit model $\mathcal{T}(p)$ was parameterized as orbital period P, inclination i, scaled semi-major axis $a/R_\star$, planet-to-star radius ratio $R_p/R_\star$, mid-transit time T_{mid}, and limb-darkening coefficients u_i, where a circular orbit was assumed. The orbital period P was fixed to 4.178062 days as reported by Lam et al. (2017). A quadratic limb-darkening law was adopted and conservatively constrained by Gaussian priors of width σ = 0.1, whose central values were calculated from the ATLAS atmosphere models following Espinoza & Jordán (2015) with stellar parameters T_{eff} = 5750 K, $\log g$ = 3.9, and [Fe/H] = −0.18.

The baseline model $\mathcal{B}(c_i)$ consisted of a selected combination of auxiliary state vectors, including spectral and spatial position drifts (x, y), the spectra full width at half maximum (FWHM) in the spatial direction (s_y), airmass (z), and time sequence (t). The Bayesian information criterion (BIC; Schwarz 1978) was used to find the baseline model that can best remove the systematics. For the white-color light curve, the model

$$\mathcal{B}_w = c_0 + c_1 s_y + c_2 z \quad (1)$$

Table 1. Derived system parameters for white light-curve analysis.

Parameter	Value
P [days]	4.178062 (fixed)
e	0 (fixed)
$T_{\rm mid}$ [BJD$_{\rm TDB}$]	2 457 808.60283 ± 0.00031
i [°]	$88.2^{+1.1}_{-0.9}$
$a/R_\star$	$7.95^{+0.19}_{-0.27}$
$R_{\rm p}/R_\star$	0.1004 ± 0.0014
u_1	0.365 ± 0.057
u_2	$0.258^{+0.88}_{-0.85}$

gave the lowest BIC value. The second-best model yields a value of ΔBIC = 3.3 higher. For the spectroscopic light-curves, the model was chosen in a semi-empirical form:

$$\mathcal{B}_{\rm spec}(\lambda) = \mathcal{S}_{\rm w} \times (c_0 + c_1 s_y(\lambda) + c_2 t + c_3 t^2), \quad (2)$$

which inherited a common-mode component $\mathcal{S}_{\rm w}$ determined from the white-color light curve. The common-mode systematics $\mathcal{S}_{\rm w}$ were derived after dividing the white-color light curve by the best-fitting transit model $\mathcal{T}(p)$.

The transit analysis package (TAP; Gazak et al. 2012), which is customized for our purposes, was employed to perform the Markov chain Monte Carlo analysis. The correlated noise was taken into account by the wavelet-based likelihood function proposed by Carter & Winn (2009). The overall transit parameters were determined from the white-color light curve, whose best-fitting values and associated uncertainties were calculated as the median and 1σ percentiles of the posterior probability distributions. The values listed in Table 1. For the spectroscopic light-curves, only the planet-to-star radius ratio $R_{\rm p}/R_\star$, the limb-darkening coefficients u_i, and the baseline coefficients c_i were fit, while the other transit parameters were fixed to the values determined from the white-color light curve. The wavelength-dependent radius ratios are presented in Table A.1. The white-color and spectroscopic light-curves are shown in Figs. 2 and A.1, respectively.

4. Results and discussion

4.1. Second-order contamination

When grism 4 is used with ALFOSC, second-order contamination can be present because different diffraction orders can overlap in the detector (Stanishev 2007). To check this problem, we performed consecutive observations of WASP-127 with grism 4 on March 21, 2017, with and without the second-order blocking filters 101 (GG475) and 102 (OG515). We find that for WASP-127, second-order contamination of the stellar flux appears at 1% level at 655 nm and rises nearly monotonically to reach 10% at 900 nm. Following the approach of Stanishev (2007), we were able to directly remove the second-order component of the blue light from the first-order stellar spectra, and then to derive a new transmission spectrum. As shown in Fig. 3, this correction makes the transit depths slightly smaller at red wavelengths ($\lambda \gtrsim 600$ nm), which agrees with the original depths well within the error bars and still shows the same relative spectral shape.

4.2. Transmission spectrum

To interpret the transmission spectrum of WASP-127b, a series of atmospheric models with an isothermal temperature structure were generated using the `Exo-Transmit` code (Kempton et al. 2017). Various metallicities, chemical compositions (with or without Na, K, TiO, and VO), and weather conditions (clear, hazy, or cloudy) were considered. We also analytically calculated a pure Rayleigh scattering model following the approach of Lecavelier Des Etangs et al. (2008), and used a simple flat straight line to represent the gray absorbing clouds.

Table 2. Goodness of fit for different atmospheric models.

Model	415–885 nm		415–655 nm	
	χ^2	$P(\chi^2)$	χ^2	$P(\chi^2)$
Pure Rayleigh scattering (RS)	22.11	0.453	4.89	0.936
Flat	18.83	0.656	8.43	0.645
1 × solar, Na/K, clear	40.41	0.010	26.59	0.005
0.1 × solar, Na/K, clear	30.64	0.104	14.71	0.196
1 × solar, Na/K/TiO/VO, 5 × RS	24.97	0.299	10.61	0.477
0.1 × solar, Na/K/TiO/VO, clear	23.95	0.350	13.40	0.268
0.1 × solar, Na/K, 5 × RS	23.29	0.386	5.79	0.887
0.1 × solar, Na/K/TiO/VO, 5 × RS	13.60	0.915	5.51	0.904
0.1 × solar, TiO/VO, 5 × RS	**11.73**	**0.963**	**4.45**	**0.955**

It is clear from Fig. 3 that the transmission spectrum is not flat, but on the contrary, has strong spectral features. It is not surprising that we can detect spectral features even using a relatively small aperture telescope, given that one atmospheric scale height, H, of WASP-127b corresponds to approximately 2500 km (equivalent to a signal of 510 ppm) assuming an H-He atmosphere, and that the amplitude of a given spectral signature can typically achieve about $5H$ (e.g., Seager 2010).

At the bluer wavelengths, the spectrum shows a decreasing slope with λ, which seems to indicate Rayleigh scattering. A hint of Na absorption is seen (although statistically insignificant), with the band centered on the Na doublet presenting a higher $R_{\rm p}/R_\star$ value than the surrounding bands. Unfortunately, the analysis of narrower passbands around Na did not provide more information but increasing noise (not shown). No K absorption is seen. Toward the red, strong absorptions from TiO and VO molecules seem to dominate the spectral shape.

Fitting the different models to the whole spectral range (415–885 nm) or the blue spectral range free of second order (415–655 nm), the model with the minimum χ^2 always includes only TiO/VO and has an enhanced Rayleigh slope, which is indicative of some haze in the atmosphere (see Fig. 3 and Table 2 for χ^2 fitting results). We find that the best-fitting models are metal poor, which is interesting because the host star is also metal poor ([Fe/H] = −0.18 ± 0.06).

Given the relatively cool equilibrium temperature of WASP-127b ($T_{\rm eq}$ = 1400 K; Lam et al. 2017), the tentative inference of the TiO/VO molecules is somewhat unexpected and intriguing. For planets with equilibrium temperatures lower than ∼1900 K, TiO could be cold trapped in the deep atmospheric layers when the temperature-pressure profile crosses the condensation curve (Showman et al. 2009; Parmentier et al. 2013, 2016). Several other possibilities could also account for the absence of TiO/VO in the upper atmosphere (Spiegel et al. 2009). Until now, only two very hot Jupiters, that is, WASP-121b ($T_{\rm eq}$ = 2400 K; Evans et al. 2016) and WASP-48b ($T_{\rm eq}$ = 1956 K; Murgas et al. 2017), have shown evidence of TiO/VO in the transmission spectrum. If the presence of TiO/VO were confirmed in the relatively "cool" atmosphere of WASP-127b, one possible scenario

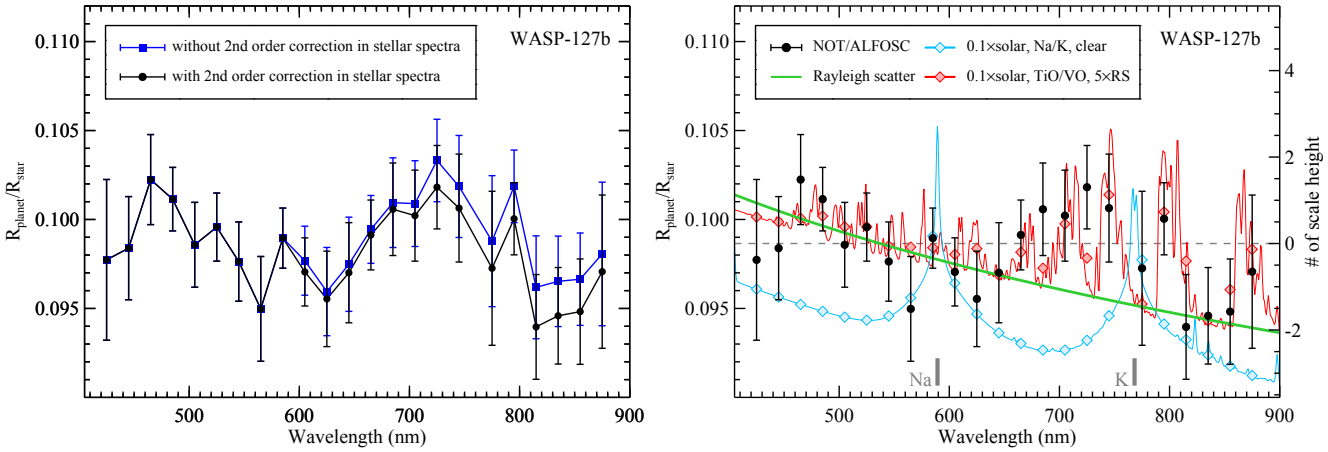

Fig. 3. NOT/ALFOSC transmission spectrum of WASP-127b, using bins 20 nm wide in wavelength. Error bars are $\pm 1\sigma$ errors. The *left panel* shows the transmission spectra with (black) or without (blue) the second-order correction in the stellar spectra. The right panel shows two 0.1 × solar atmospheric models computed using `Exo-Transmit` (Kempton et al. 2017, red model: with TiO/VO, but without Na/K, 5× Rayleigh scattering, sky-blue model: with Na/K, but without TiO/VO, clear), and a pure Rayleigh slope, together with the corrected transmission spectrum.

to avoid the cold trap could be that the stellar irradiation is directly deposited into the deeper interior of WASP-127b, thereby changing the deep temperature profile (e.g., Perna et al. 2010; Batygin & Stevenson 2010; Batygin et al. 2011; Huang & Cumming 2012; Rauscher & Menou 2013; Spiegel & Burrows 2013; Lopez & Fortney 2016.

5. Conclusions

We have observed one transit of WASP-127b, an inflated, sub-Neptune mass planet. Because of its low density, the observed atmospheric scale height signals are strong, and we were even able to retrieve its transmission spectrum with the NOT telescope. After considering the possible effects of second-order contamination in the spectra, the spectrum shows a strong Rayleigh-like slope at blue wavelengths and a hint of Na absorption, although the quality of the data does not allow us to claim a detection. At redder wavelengths the absorption features of TiO and VO are the best explanation to fit the observed data. While the S/N is low, these findings are enough to conclude that the atmosphere of WASP-127b is either completely or partially cloud free.

The brightness of its host star, which is a close-by comparison star, together with its extraordinary inflation and its short period all contribute to make WASP-127b a prime target for further follow-up with ground- and space-based facilities, including the JWST, which will be able to confirm our findings and extend them into the infrared regime. Finding the physical mechanism(s) responsible for this inflation will help us understand how this type of planets evolves and how their fate is tied to that of their host star.

Acknowledgements. This article is based on observations made in the Observatorios de Canarias del IAC with the NOT telescope operated on the island of La Palma by the NOTSA in the Observatorio del Roque de los Muchachos (ORM). This work is partly financed by the Spanish MINECO through grants ESP2013-48391-C4-2-R, and ESP2014-57495-C2-1-R. G.C. acknowledges the support by the National NSF of China (Grant No. 11503088) and the Nat. Sci. Found. of Jiangsu Province (Grant No. BK20151051). DLP is supported by the UK's STFC and a Royal Society Wolfson Merit award.

References

Bailey, J. 2014, PASA, 31, e043
Batygin, K., & Stevenson, D. J. 2010, ApJ, 714, L238
Batygin, K., Stevenson, D. J., & Bodenheimer, P. H. 2011, ApJ, 738, 1
Bean, J. L., Miller-Ricci Kempton, E., & Homeier, D. 2010, Nature, 468, 669
Carter, J. A., & Winn, J. N. 2009, ApJ, 704, 51
Charbonneau, D., Brown, T. M., Noyes, R. W., & Gilliland, R. L. 2002, ApJ, 568, 377
Chen, G., Guenther, E. W., Pallé, E., et al. 2017a, A&A, 600, A138
Chen, G., Palle, E., Murgas, F., et al. 2017b, A&A, submitted
Chen, G., Pallé, E., Nortmann, L., et al. 2017c, A&A, 600, L11
Eastman, J., Siverd, R., & Gaudi, B. S. 2010, PASP, 122, 935
Espinoza, N., & Jordán, A. 2015, MNRAS, 450, 1879
Evans, T. M., Sing, D. K., Wakeford, H. R., et al. 2016, ApJ, 822, L4
Fortney, J. J., & Nettelmann, N. 2010, Space Sci. Rev., 152, 423
Fortney, J. J., Marley, M. S., & Barnes, J. W. 2007, ApJ, 659, 1661
Gazak, J. Z., Johnson, J. A., Tonry, J., et al. 2012, Adv. Astron., 2012, 30
Guillot, T. 2005, Ann. Rev. Earth Planet. Sci., 33, 493
Horne, K. 1986, PASP, 98, 609
Howard, A. W., Marcy, G. W., Bryson, S. T., et al. 2012, ApJS, 201, 15
Huang, X., & Cumming, A. 2012, ApJ, 757, 47
Kempton, E. M.-R., Lupu, R. E., Owusu-Asare, A., Slough, P., & Cale, B. 2017, PASP, 129, 044402
Lam, K. W. F., Faedi, F., Brown, D. J. A., et al. 2017, A&A, 599, A3
Lammer, H., Erkaev, N. V., Odert, P., et al. 2013, MNRAS, 430, 1247
Lecavelier Des Etangs, A., Vidal-Madjar, A., Désert, J.-M., & Sing, D. 2008, A&A, 485, 865
Leconte, J., Chabrier, G., Baraffe, I., & Levrard, B. 2010, A&A, 516, A64
Lopez, E. D., & Fortney, J. J. 2016, ApJ, 818, 4
Madhusudhan, N., Amin, M. A., & Kennedy, G. M. 2014, ApJ, 794, L12
Madhusudhan, N., Agúndez, M., Moses, J. I., & Hu, Y. 2016, Space Sci. Rev., 205, 285
Mandel, K., & Agol, E. 2002, ApJ, 580, L171
Mazeh, T., Holczer, T., & Faigler, S. 2016, A&A, 589, A75
Mousis, O., Lunine, J. I., Madhusudhan, N., & Johnson, T. V. 2012, ApJ, 751, L7
Murgas, F., Pallé, E., Zapatero Osorio, M. R., et al. 2014, A&A, 563, A41
Murgas, F., Palle, E., Chen, G., et al. 2017, A&A, submitted
Nortmann, L., Pallé, E., Murgas, F., et al. 2016, A&A, 594, A65
Öberg, K. I., Murray-Clay, R., & Bergin, E. A. 2011, ApJ, 743, L16
Parmentier, V., Showman, A. P., & Lian, Y. 2013, A&A, 558, A91
Parmentier, V., Fortney, J. J., Showman, A. P., Morley, C., & Marley, M. S. 2016, ApJ, 828, 22
Parviainen, H., Pallé, E., Nortmann, L., et al. 2016, A&A, 585, A114
Perna, R., Menou, K., & Rauscher, E. 2010, ApJ, 719, 1421
Rauscher, E., & Menou, K. 2013, ApJ, 764, 103
Schwarz, G. 1978, Annals of Statistics, 6, 461
Seager, S. 2010, Exoplanet Atmospheres: Physical Processes (Princeton University Press)
Showman, A. P., Fortney, J. J., Lian, Y., et al. 2009, ApJ, 699, 564
Sing, D. K., Fortney, J. J., Nikolov, N., et al. 2016, Nature, 529, 59
Snellen, I. A. G., de Kok, R. J., de Mooij, E. J. W., & Albrecht, S. 2010, Nature, 465, 1049
Spiegel, D. S., & Burrows, A. 2013, ApJ, 772, 76
Spiegel, D. S., Silverio, K., & Burrows, A. 2009, ApJ, 699, 1487
Stanishev, V. 2007, Astron. Nachr., 328, 948
Wu, Y., & Lithwick, Y. 2013, ApJ, 763, 13

Appendix A: Spectro-photometric data

Observed color light curves are shown in Fig. A.1, and the derived transit depths at each spectral pass band are given here in Table A.1.

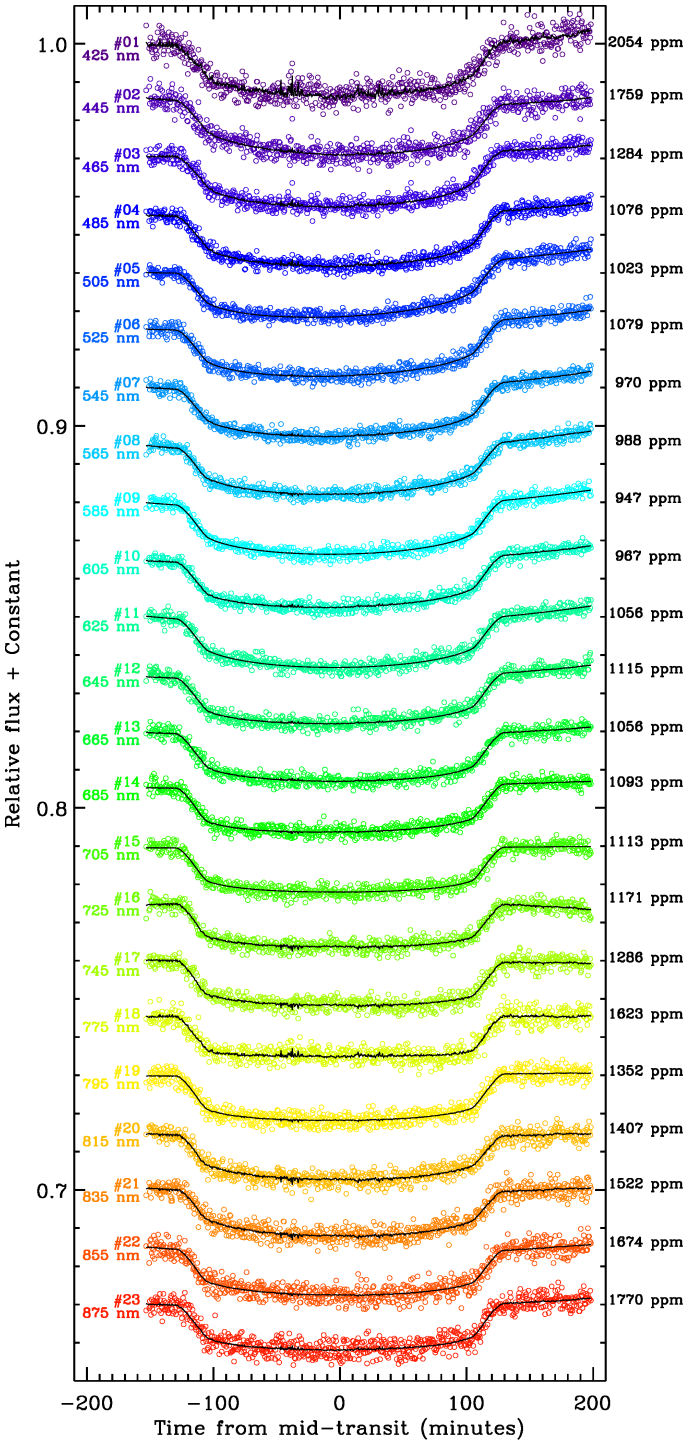

Fig. A.1. Spectroscopic light-curves of WASP-127 and the best-fitting models after the common-mode systematics have been removed.

Table A.1. Transmission spectrum values obtained with NOT/ALFOSC.

#	Wavelength (nm)		$R_p/R_\star$	$R_p/R_\star$
	Center	Width	(With 2nd order)	(Corrected)
1	425	20	0.0977 ± 0.0045	0.0977 ± 0.0045
2	445	20	0.0984 ± 0.0029	0.0984 ± 0.0029
3	465	20	0.1022 ± 0.0025	0.1022 ± 0.0025
4	485	20	0.1011 ± 0.0018	0.1011 ± 0.0018
5	505	20	0.0986 ± 0.0024	0.0986 ± 0.0024
6	525	20	0.0996 ± 0.0019	0.0996 ± 0.0019
7	545	20	0.0976 ± 0.0022	0.0976 ± 0.0022
8	565	20	0.0950 ± 0.0029	0.0950 ± 0.0029
9	585	20	0.0990 ± 0.0017	0.0990 ± 0.0017
10	605	20	0.0977 ± 0.0019	0.0971 ± 0.0019
11	625	20	0.0959 ± 0.0025	0.0955 ± 0.0027
12	645	20	0.0975 ± 0.0026	0.0970 ± 0.0028
13	665	20	0.0994 ± 0.0019	0.0991 ± 0.0020
14	685	20	0.1009 ± 0.0025	0.1006 ± 0.0026
15	705	20	0.1009 ± 0.0024	0.1002 ± 0.0026
16	725	20	0.1033 ± 0.0023	0.1018 ± 0.0023
17	745	20	0.1019 ± 0.0029	0.1006 ± 0.0030
18	775	20	0.0988 ± 0.0037	0.0973 ± 0.0043
19	795	20	0.1019 ± 0.0020	0.1000 ± 0.0020
20	815	20	0.0962 ± 0.0029	0.0940 ± 0.0029
21	835	20	0.0965 ± 0.0025	0.0946 ± 0.0027
22	855	20	0.0966 ± 0.0026	0.0948 ± 0.0030
23	875	20	0.0981 ± 0.0040	0.0971 ± 0.0043